First evidence of Alfvén wave activity in KSTAR plasmas

2013 Plasma Phys. Control. Fusion 55 045004

(http://iopscience.iop.org/0741-3335/55/4/045004)

Plasma Phys. Control. Fusion **55** (2013) 045004 (6pp) doi:10.1088/0741-3335/55/4/045004

First evidence of Alfvén wave activity in KSTAR plasmas

M J Hole[1], C M Ryu[2], M H Woo[3], J G Bak[3], S E Sharapov[4], M Fitzgerald[1] and the KSTAR Team[3]

[1] Research School of Physical Sciences and Engineering, Australian National University, Acton 0200, ACT Australia
[2] POSTECH, Pohang, Korea
[3] National Fusion Research Institute, Daejeon, Korea
[4] EURATOM/CCFE Fusion Assoc., Culham Science Centre,Abingdon, Oxon OX14 3DB, UK

Received 18 June 2012, in final form 30 January 2013
Published 22 February 2013
Online at stacks.iop.org/PPCF/55/045004

Abstract
We report on first evidence of wave activity during neutral beam heating in KSTAR plasmas: 40 kHz magnetic fluctuations with a toroidal mode number of $n = 1$. Our analysis suggests this a beta-induced Alfvén eigenmode (BAE) resonant with the $q = 1$ surface. A kinetic analysis, when coupled with electron temperature measurements from electron cyclotron emission and ion/electron temperature ratios from crystallography, enables calculation of the frequency evolution, which is in agreement with observations. Complementary detailed magnetohydrodynamic (MHD) modelling of the magnetic configuration and wave modes supports the BAE conclusion, by locating an $n = 1$ mode separated from the continuum in the core region. Finally, we have computed the threshold to marginal stability for a range of ion temperature profiles. These suggest the BAE can be driven unstable by energetic ions when the ion temperature radial gradient is sufficiently large. Our findings suggest that mode existence could be used as a form of inference for temperature profile consistency in the radial interval of the mode, thereby extending the tools of MHD spectroscopy.

(Some figures may appear in colour only in the online journal)

1. Introduction

Instabilities such as Alfvén eigenmodes, driven by fast particles, are of programmatic concern as they can expel energetic ions from the plasma, thereby preventing heating by thermalization [1]. In addition, such energetic particles expelled can damage the first wall, and a fusion reactor can only tolerate fast particle losses of a few per cent [2]. Another motivation for the study of Alfvén eigenmodes is their potential use as a diagnostic for the plasma, particularly through the tool of magnetohydrodynamic (MHD) spectroscopy [3].

One such class of fast particle-driven instabilities that can occur at relatively low frequency are beta-induced Alfvén eigenmodes (BAEs). The characteristic experimental features of this instability are magnetic fluctuations at a frequency intermediate between the fishbone and the toroidal Alfvén eigenmode (TAE), with angular frequency $\omega_{\mathrm{TAE}} = v_{\mathrm{A}}/(2qR)$, with v_{A} the Alfvén speed, q the safety factor and R the major radius [4]. These modes were first identified in DIII-D [5], and have since been discovered in other tokamaks in beam [6], ion cyclotron heated [7] and Ohmically heated discharges in the presence of a magnetic island [8–12]. More advanced kinetic treatments, which include corrections to kinetic theory for diamagnetic and shaping effects, as well as the inclusion of trapped particles have been used to study BAEs in ASDEX [13]. Radial profile information was measured during sawteeth in Tore Supra [14]. Recently, BAEs driven by electron populations have been observed in the tokamak HL-2A [15], and it is possible that energetic electrons are responsible for driving Alfvénic magnetic oscillations in the H-1 heliac [16].

The aim of this paper is to report on first evidence of Alfvénic wave activity during neutral beam heating in KSTAR plasmas. In 2010 and 2011 campaigns KSTAR plasmas included 1.2 MW of neutral beam heating, which provided a source of heating to excite Alfvénic wave activity modes. Data from the 2010 campaign, which was fully analysed during 2011, show 40–60 kHz magnetic fluctuations. We present the first ideal MHD calculation of a core localized

mode with toroidal mode number $n = 1$ for an experimental configuration. The mode is global with very small resonance with continuum modes. Second, this work is the first observation of Alfvénic wave activity in KSTAR. With up to 14 MW of neutral beam heating and 14 MW of RF heating planned, KSTAR plasmas will become a pilot for ITER plasmas, and provide the opportunity to explore the wave–particle–plasma interaction in regimes approaching burning plasmas. Our work builds on preliminary observations of electron fishbones in KSTAR in 2009 [17], and aliased TAE activity in 2011 [18]. Finally, as a spin-off, we have developed a new form of MHD spectroscopy for consistency of the temperature profile with the observation of wave activity. The rest of the work is as follows: in section 2 we introduce the experiments conducted in KSTAR, and in section 3 present detailed modelling. Section 4 contains concluding remarks and discusses implications for future work.

2. Experiments

In 2010 a set of neutral beam injection (NBI) excitation experiments were conducted in KSTAR in an attempt to generate shear Alfvénic wave activity. Subject to operator controls, the choice of plasma conditions were optimized for this purpose: a relatively low toroidal magnetic field of 1.95 T, and maximum available NBI heating: 1.2 MW of 80 keV NBI. For deuterium plasmas, 80 keV NBI would produce fast D neutrals with speed $v_{||,\mathrm{beam}} = 2.8 \times 10^6\,\mathrm{m\,s^{-1}}$. With plasma densities of up to $5 \times 10^{19}\,\mathrm{m^{-3}}$ expected, the minimum Alfvén speed is $v_\mathrm{A} = 4.4 \times 10^6\,\mathrm{m\,s^{-1}}$. While the beam speed is sub-Alfvénic, it is greater than the first sideband resonance at $v_\mathrm{A}/3$, and so it is possible that TAEs may be excited, as was found during early operation of MAST [19]. Alfvén cascades have also been observed on JET in reverse shear configurations with $v_{||,\mathrm{beam}}/v_\mathrm{A}$ as low as 0.2 [20].

Four NBI heated discharges (#4218-#4220) were produced, with flat top plasma current I_p in the range $210 < I_\mathrm{p} < 407$ kA, electron cyclotron resonance heating (ECRH) power up to 200 kW, and core-plasma density up to $3 \times 10^{19}\,\mathrm{m^{-3}}$. There was no discernible impact of ECRH heating on these plasmas. Figure 1 shows the temporal evolution of one such discharge, #4220. For this 4.5 s plasma, 2 s of NBI was applied from 2 s during current flat-top.

Figure 2 shows magnetic oscillations of discharge #4220. The mode activity correlated with NBI heating, and a study of electron cyclotron emission data reveals that the plasma is sawtoothing throughout the heating phase. A study of signal phase versus geometric angle, computed from a toroidal Mirnov array provides weak evidence that the mode has $n = 1$. Unfortunately, the coils are located flush with the conducting wall, and so the signal-to-noise ratio is large, and there is significant $n = 0$ noise present. Information about the poloidal mode number is not available. Similar oscillations were observed in discharges #4218, #4219 and #4221.

A simple scoping exercise reveals that the mode activity is unlikely to correspond to a TAE. The middle of the TAE gap lies at $\omega_\mathrm{TAE} = v_\mathrm{A}/(2qR)$. Using $n_\mathrm{i} \approx n_\mathrm{e}(0)$, taking R as the magnetic axis, and using $q = q_{mn} = (2m + 1)/(2n)$ for

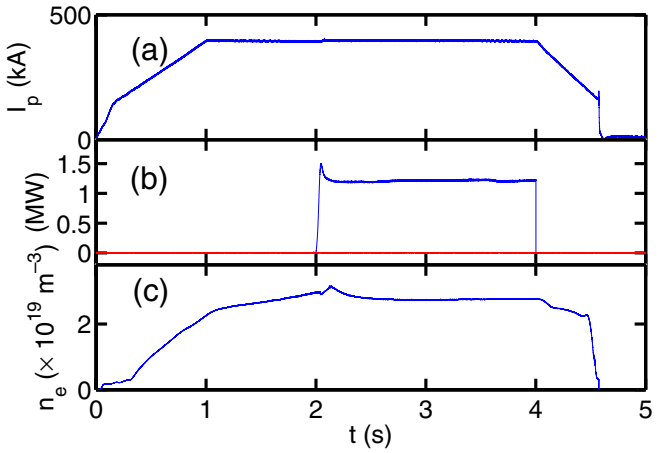

Figure 1. Evolution of #4220 showing (*a*) plasma current I_p, (*b*) auxiliary heating (P_NBI in blue, P_ECRH in red) and (*c*) line-averaged electron density n_e.

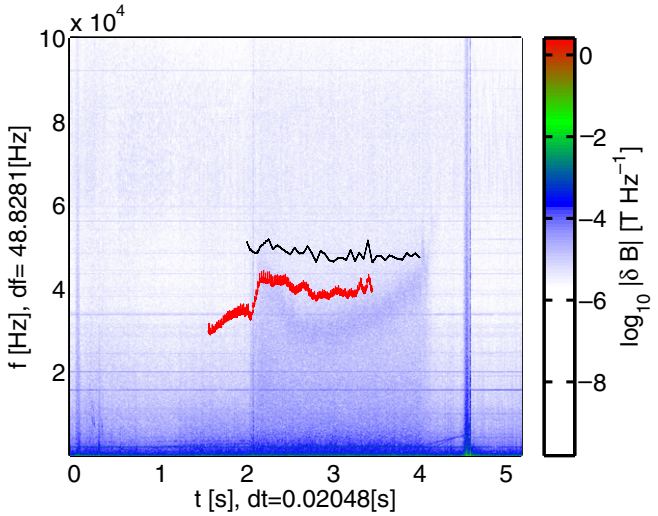

Figure 2. Magnetic spectrogram of #4220 with ω_CAP (red) and BAE (black) from figure 5(*a*) overlaid (red).

$m = 1, 2, 3$ gives 160 kHz, 100 kHz and 70 kHz, respectively. Mode activity with frequency of order 150 kHz and $m = n = 1$ was observed in the 2011 campaign. The observed mode reported here has a frequency of 40 kHz, which would be commensurate with a resonance of $q = 5$. This is the edge q of these elongated plasmas, and so the TAE frequency will be significantly greater than 40 kHz due to the lower edge density. Following Gorelenkov *et al* [21] we have also computed the thermal ion transit frequency $\omega_\mathrm{ti} = \sqrt{2k_\mathrm{B}T_\mathrm{i}/m_\mathrm{i}}\,/\,(qR_0)$, which is the upper beta-acoustic Alfvén Eigenmode (BAAE) gap frequency. For KSTAR plasmas, the on-axis frequency ranges from 29 kHz, using the central ion temperature inferred from #4229 down to 17 kHz. These are below the observed wave frequency, at 40–60 kHz.

In contrast, the frequency as well as its time evolution is a closer match to the evolution of the kinetic accumulation frequency $\omega_\mathrm{CAP} = 1/R_0\sqrt{2T_\mathrm{i}/m_\mathrm{i}(7/4 + T_\mathrm{e}/T_\mathrm{i})}$, with R_0 the major radius, m_i the ion mass, and T_i and T_e the ion and electron temperatures, respectively [22]. Electron cyclotron emission (ECE) data gives the on-axis value of electron temperature

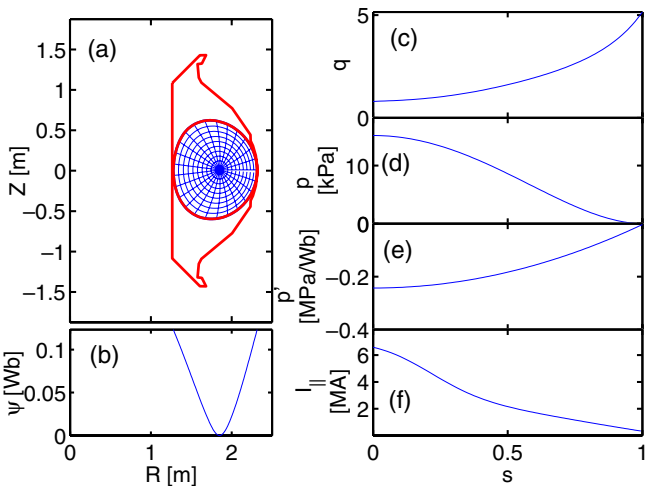

Figure 3. Equilibrium for #4220 at 2 s. (*a*) shows contours of poloidal flux with the plasma vessel cross section overlaid, and (*b*) is a major radius profile of poloidal flux ψ. Panels (*c*)–(*f*) show q, p, $p'(\psi)$ and $I_{||}$ as a function of s, the square root of normalized poloidal flux.

$T_e = 1.2$ keV. While not available for discharge #4220, x-ray imaging crystal spectrometer [23] data providing T_i, T_e is available for nearby discharge #4229 with the same level of NBI heating. This pulse also shows evidence of toroidal rotation, with core rotation up to 100 km s^{-1}, producing a core Doppler shift of up to 8kHz. Rotation of either a near stationary mode or magnetic island is thus insufficient to describe the observations.

Correcting for the offset in neutral beam heating interval for this discharge, we have computed ω_{CAP} and over plotted the evolution in figure 2. The frequency match is close, as is the slight frequency drop following beam turn-on at 2 s. The drop in frequency occurs due to the initial drop in $T_e$observed in the core ECE channel. Similar BAE frequency scaling is evident for discharges #4218 and #4219.

3. Detailed modelling

We have undertaken detailed modelling of the plasma at the onset of mode activity at 2 s. By analysing data from a set of 20 ECE chords we have been able to identify the inversion radius and locate the $q = 1$ surface. To correct the $q = 1$ surface of magnetics-only constrained EFIT to match ECE data we have used CHEASE [24] to remap the current profile as $I^*(s) \rightarrow I^*(s) + cI_{core}(s)$ and pressure profile with $p'(s) \rightarrow \lambda p'(s)$ so as to match the sawtooth inversion radius and EFIT β_p, respectively. Here, s is the square root of normalized poloidal flux, with $s = 0$ the core and $s = 1$ the edge. The core current profile selected is a ramp, $I_{core}(s) = 1 - s$. Figure 3 shows a cross section of the corrected equilibrium flux surfaces and q profile.

Figure 4 shows the Alfvén and ion sound continuum for $n = 1$, computed using the code CSCAS [25] with adiabatic index $\gamma = 5/3$. In figure 4(*a*) the toroidicity- and ellipticity-induced gaps can be identified. Using the most recent version of the ideal MHD global stability code MISHKA [26] we have computed TAE gap modes. The TAE gap mode produced by the $q_{mn} = (2m + 1)/2n = 1.5$ resonance at $s = 0.45$ has a frequency of 120 kHz, well above the measured 40 kHz oscillation. In figure 4(*b*) we have zoomed into the low-frequency part of the continuum and identified different continuum branches. As shown by Gorelenkov *et al* [21], the frequency of the ion sound and modified shear Alfvén continuum modes drops to zero at rational surfaces. The accumulation point of the low-frequency gap introduced in the shear-Alfvén continuous spectrum because of finite beta is $\omega_{As,gap}/\omega_A = (\gamma\beta)^{0.5}$, with ω_A the Alfvén angular frequency at the magnetic axis. To identify a global mode separated from the MHD continuum, we have selected an s interval of $0 < s < 0.3$, thereby avoiding the resonance with the $m = 3$ ion sound branch. The discrete mode identified in figure 4(*b*) is separated from the continuum above and below, and so forms a gap mode between singular modes. In the limit that the s interval is expanded to the full domain, the eigenfunction retains its global structure. The mode frequency is $\omega/\omega_A = -0.1371$. A single-channel millimetre-wave interferometer system provides a measurement of the time-resolved line-integrated electron density, n_e [27]. Assuming a parabolic profile for the density provides a measure of on-axis density. If $n_i \approx 0.8n_e$ is also assumed [28], the Alfvén angular frequency can be computed, yielding $\omega/(2\pi) \approx 50$ kHz at 2 s. We have overplotted the frequency evolution of this estimate in figure 2.

The mode, which is resonant with the core of the plasma, has similar global mode structure to modes computed in DIII-D by Turnbull *et al* [29]. In contrast, the BAE modelled by Huysmans *et al* [30] is in the region of greater shear, and possesses more poloidal harmonics. Figure 5 shows the V_1 eigenvector, which is the ρ component of the contravariant fluid displacement velocity, for (*a*) a discrete mode, and (*b*) a nearby continuum mode. A continuum mode is one that is localized to a resonant surface with poloidal flux ψ, and a solution of the shear Alfvén dispersion relation $\omega(\psi) = k_{||}(\psi)v_A(\psi)$, with $k_{||} = \boldsymbol{k} \cdot \boldsymbol{B}/B$ [25]. The BAE in figure 5(*a*) has a global mode structure with negligent resonant coupling with continuum modes, whereas the continuum mode in figure 5(*b*) has resonances at crossings of the continuum at $s = 0.57, s = 0.66$ for $m = 2$ and $s = 0.77, s = 0.84$ for $m = 3$. In contrast to earlier work [29, 30], the global mode of figure 5(*a*) has significantly reduced coupling to resonances with the continuum, and therefore will exhibit weaker continuum damping.

Ideal MHD codes such as MISHKA solve for the wave structure in full toroidal geometry, but provide no information about mode drive. The particle–wave resonance condition [31] is

$$\frac{n}{R}v_{||} - \frac{m+l}{qR}v_{||} - \omega = 0, \qquad (1)$$

where l is a Fourier mode number in poloidal angle θ of the particle magnetic drift velocity. The mode peaks at $s = 0.16$, for which $q = 0.89$. At this radial location the $l = 0$ resonance condition requires the unphysical condition $v_{||}/v_{||,beam} = 1.3$, while for $|l| \geqslant 1$ the resonance condition can be satisfied for

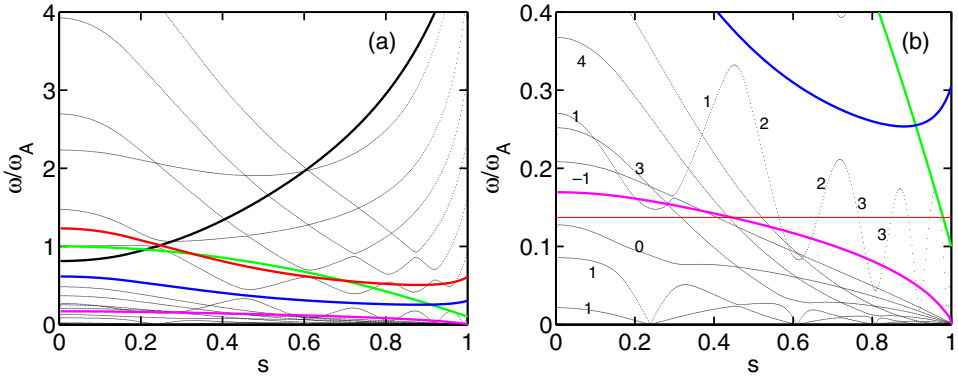

Figure 4. Ion sound and Shear Alfvén continuum (shown as black points) for $n = 1$ modes for #4220 at 2 s. Also shown is the q profile (solid black curve), normalized mass density profile ρ/ρ_0 (solid green curve), TAE frequency (solid blue curve), elliptical Alfvén eigenmode frequency (solid red curve) and accumulation point of the low-frequency gap $\omega_{\mathrm{As,gap}}$ (solid pink curve). (b) focuses on the BAE region, which also shows the BAE (red line).

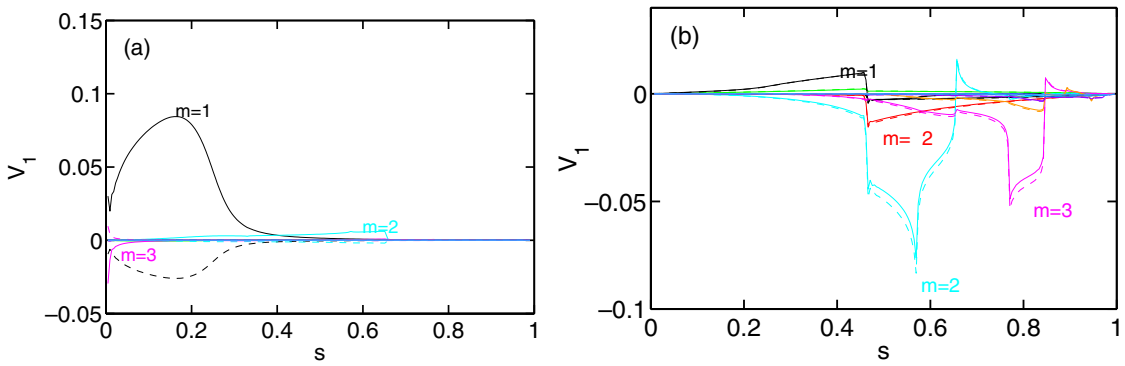

Figure 5. Eigenfunctions for (a) an $n = 1$ BAE with frequency $\omega/\omega_{\mathrm{A}} = -0.1371$, and ($b$) an $n = 1$ continuum mode with frequency $\omega/\omega_{\mathrm{A}} = -0.1380$. Both real (solid) and imaginary (dashed) components are shown.

$v_{||} < v_{||,\mathrm{beam}}$. Thus, the mode can be driven by the fundamental resonance at $|l| = 1$ [22], as well as by sidebands, $|l| > 1$. The mode resonance is broad due to the finite radial region of varying q covered by the mode width.

Meanwhile, the mode excitation threshold by energetic ions is reduced by inverse ion Landau damping connected with finite thermal ion temperature gradient [22]. In the limit of vanishing continuum damping, an estimate of the threshold to marginal stability can be made using the kinetic treatment of Zonca *et al* [22], which studied the drive due to thermal ion temperature radial gradients, and studied the relationship between kinetic ballooning modes (KBMs) and BAEs. In that treatment it was shown the stability conclusions were a function of the frequency range of ω_{CAP} relative to the core-plasma ion diamagnetic frequency $\omega_{*\mathrm{pi}} = (k_{\mathrm{B}}T_{\mathrm{i}}/e_{\mathrm{i}}B)(\boldsymbol{k}\times\boldsymbol{b})\cdot\nabla\ln P_{\mathrm{i}}$. Here, k_{B} is Boltzmann's constant, $\boldsymbol{k} = m/r\boldsymbol{e}_\theta + n/R\boldsymbol{e}_\phi$ the wave vector, $\boldsymbol{b} = \boldsymbol{B}/|\boldsymbol{B}|$, and P_{i} the thermal ion pressure. If $\omega^2_{*\mathrm{pi}} \ll \omega^2_{\mathrm{CAP}}$ the KBM accumulation point was always stable, and the BAE may become unstable for values of $\eta_{\mathrm{i}} = (\partial\ln T_{\mathrm{i}}/\partial\ln n_{\mathrm{i}})$ greater than a critical value η_{ic}, given by

$$\eta_{\mathrm{ic}} \approx \frac{2}{\sqrt{7+4\tau}}\frac{\omega_{\mathrm{ti}}}{q\omega_{*\mathrm{ni}}}, \tag{2}$$

with $\omega_{*\mathrm{ni}} = (k_{\mathrm{B}}T_{\mathrm{i}}/e_{\mathrm{i}}B)(\boldsymbol{k}\times\boldsymbol{b})\cdot\nabla n_{\mathrm{i}}/n_{\mathrm{i}}$ the ion diamagnetic drift frequency. If $\omega_{*\mathrm{pi}}$ is increased further, the unstable BAE accumulation point is expected to smoothly connect to an unstable KBM accumulation point with exponentially small growth rate when $\omega^2_{*\mathrm{pi}} \gg \omega_{\mathrm{CAP}}$. The most unstable BAE/KBM accumulation point occurs when $\omega^2_{*\mathrm{pi}} \approx \omega^2_{\mathrm{CAP}}$, when the BAE and KBM are strongly coupled. For the plasma conditions of KSTAR, we compute $\omega_{*\mathrm{pi}}/(2\pi) \approx 4$ kHz, and so $\omega^2_{*\mathrm{pi}} \ll \omega^2_{\mathrm{CAP}}$, and thus plasmas with $\eta > \eta_{\mathrm{ic}}$ with η_{ic} given by equation (2) are unstable. In this frequency regime $\delta E_{\|} \approx 0$, consistent with ideal MHD. Indeed, we compute $\omega_{\mathrm{As,gap}}/(2\pi) \approx 60$ kHz at the minimum of the $m = 1$ continuum at $s = 0.24$. This frequency, and the computed BAE gap mode frequency of 50 kHz at 2 s, is close to the kinetic accumulation frequency ω_{CAP}.

By expanding $\eta_{\mathrm{i}} = (\partial\ln T_{\mathrm{i}}/\partial\ln n_{\mathrm{i}}) = \frac{\partial\ln T_{\mathrm{i}}}{\partial r}/\frac{\partial\ln n_{\mathrm{i}}}{\partial r}$, as well as $(\boldsymbol{k}\times\boldsymbol{b})\cdot\nabla n_{\mathrm{i}}/n_{\mathrm{i}} = (\boldsymbol{k}\times\boldsymbol{b})_r\frac{\partial\ln n_{\mathrm{i}}}{\partial r}$, the ratio $\eta_{\mathrm{i}}/\eta_{\mathrm{ic}}$ expands as

$$\eta_{\mathrm{i}}/\eta_{\mathrm{ic}} = \frac{\partial\ln T_{\mathrm{i}}}{\partial r}\frac{k_{\mathrm{B}}T_{\mathrm{i}}/(e_{\mathrm{i}}B)(\boldsymbol{k}\times\boldsymbol{B})_r}{\sqrt{2/(7+4\tau)}\omega_{*\mathrm{i}}/q}. \tag{3}$$

Equation (3) is independent of the ion density profile, and so can be computed for different radial temperature profiles.

X-ray crystallography of nearby discharge #4229 measures $T_{\mathrm{i}}(0)/T_{\mathrm{e}}(0) = 0.75$ during NBI heating, and we have used this value for #4220. Together with ECE T_{e} data for #4220, this fixes T_{i} on-axis. To account for the unknown core localization of the ion temperature profile, we have expressed the temperature profile as the sum of profiles $T_{\mathrm{a}}(s)$ and $T_{\mathrm{b}}(s)$,

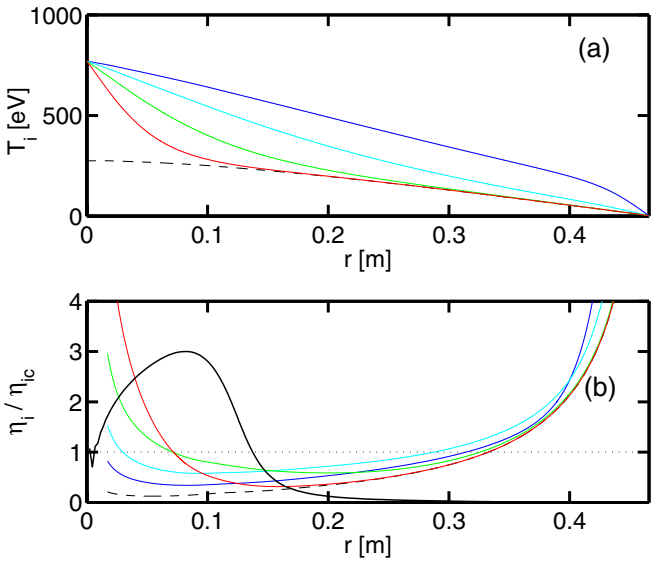

Figure 6. Variation of η_i/η_{ic} threshold with different ion temperature profiles. (*a*) shows possible ion temperature profiles (solid) with core temperature matching crystallography data from discharge #4229, and (*b*) shows the corresponding profile of η_i/η_{ic} . In both panels the dashed line corresponds to a possible Ohmic ion temperature profile, with τ taken from discharge #4229 prior to NBI heating. In (*b*) the light line is $|V_1|$ of the BAE in figure 5(*a*).

with $T_i(s) = T_a(s) + T_b(s)$, and $r \approx sa$, with a the minor radius. The profile $T_a(s)$ is an approximation to the Ohmic temperature profile. A constraint for $T_a(0)$ is provided by crystallography during the pre-NBI heating phase of #4229: that is $T_a(0) = 0.25T_e(0)$. As a plausible estimate for the Ohmic ion temperature profile we have assumed $n(s) \propto T_a(s)$, and inferred $T_a(s)$ from the equilibrium pressure profile. Finally, we have modelled the core temperature profile as

$$T_b(s) = (T_i(0) - T_a(0))(1 - \tanh(\alpha s))\tanh(10(1 - s)), \quad (4)$$

with α varied to control the core radial localization of $T_b(s)$, and term $\tanh(10(1 - s))$ included to force $T_b(s)$ to zero at $s = 1$.

Figure 6(*a*) shows a plot of different candidate modelled ion temperature profiles on the outboard radial chord, and figure 6(*b*) shows the corresponding η_i/η_{ic} values. The candidate BAE in figure 5(*a*), whose $m = 1$ Fourier magnitude is also shown in figure 6(*b*), has a peak at radial position $r \approx 0.08$ m with a radial width of $0.2a = 0.1$ m. For this mode, $\eta_i/\eta_{ic} < 1$ for a broad, Ohmic-like ion temperature profile. For sufficiently high radial temperature gradient and/or sufficiently high ion temperature, the Alfvénic ion temperature gradient driven mode [22] instability threshold will be approached, or possibly even exceeded, in the region where the mode amplitude is large, and so the mode can become unstable, due to a combination of energetic and thermal ion kinetic effects [32].

4. Conclusions

We have provided first evidence of beta-induced Alfvén eigenmode activity in neutral beam heated KSTAR plasmas. The 40 kHz, $n = 1$ observed mode matches the frequency of the accumulation point of the Alfvén continuum. Using the radial localization of sawtooth inversion radius, we have been able to identify the radial position of the $q = 1$ surface, and using this, constrain the equilibrium. A detailed mode analysis reveals the presence of a core localized beta-induced Alfvén eigenmode. Finally, a kinetic treatment of the mode marginal stability threshold shows a range of plausible ion temperature profiles for which the mode exctiation threshold is reduced, and the mode can be driven by energetic ions. This suggests that mode existence could be used as a form of inference for temperature profile consistency in the radial interval of the mode, once beam drive and relevant damping contributions have been computed, thereby extending the tools of MHD spectroscopy. Our suggestion is complementary to recent work by Bertram *et al* [33], who suggested mode frequency could be used to infer the temperature at the resonant surface of a BAE in the H-1 heliac.

Improvements in diagnosis and reliability of KSTAR plasmas will enable further exploration of new physics, in steady-state plasma environments of up to 14 MW of NBI heating. A priority is the introduction of kinetic and motional Stark effect constraints to EFIT, which will remove uncertainties in detailed modelling. In future work we hope to consolidate mode frequency variation with pressure and magnetic field strength. Judicious phasing of NBI during current ramp-up and ramp-down, together with new electron cyclotron current drive systems also offers the opportunity to influence the magnetic field configuration through co- and counter-injection. A wider sample set of modes, together with concurrent crystallography data, would enable a more thorough investigation of marginal stability thresholds and a quantitative study of mode drive and damping. Finally, as the position of the resonances are determined by the q profile and the density profile, similarity experiments with different edge q profiles and density profiles would illuminate the level of continuum damping. For instance, as the q profile flattens different m continuum mode branches are removed, and continuum damping is reduced. Alternately, as the density profile in the edge drops the location of the continuum resonance moves inwards. In this case the radial separation between the resonances and gap mode decreases, the coupling of the eigenfunction to the continuum becomes stronger, and hence the continuum damping is increased [34, 35].

Acknowledgments

This work was partly funded by the Australian Government through Australian Research Council grants FT0991899, DP1093797, as well as National Research Foundation of Korea grants NFR-2008-0062-209 and NRF-2011-0026107 and the RCUK Energy Programme under grant EP/I501045 and the European Communities under the contract of Association between EURATOM and CCFE. The views and opinions expressed herein do not necessarily reflect those of the European Commission. The authors gratefully acknowledge the support of J Kim from NFRI in assisting with access to KSTAR data, and the support of G A Huysmans from CEA Cadarache in the provision of CSCAS, HELENA and MISHKA codes.

References

[1] Breizman B N and Sharapov S E 2011 Major minority: energetic particles in fusion plasmas *Plasma Phys. Control. Fusion* **53** 054001

[2] Pinches S D *et al* and JET-EFDA Contributors 2004 The role of energetic particles in fusion plasmas *Plasma Phys. Control. Fusion* **46** B187–200

[3] Holties H A, Fasoli A, Goedbloed J P, Huysmans G T A and Kerner W 1997 Determination of local tokamak parameters by magnetohydrodynamic spectroscopy *Phys. Plasmas* **4** 709–19

[4] Heidbrink W W, Ruskov E, Carolipio E M, Fang J and van Zeeland M A 1999 What is the beta-induced Alfvén eigenmode? *Phys. Plasmas* **6** 1147–61

[5] Heidbrink W W, Strait E J, Chu M S and Turnbull A D 1993 Observation of beta-induced Alfvén eigenmodes in the DIII-D tokamak *Phys. Rev. Lett.* **71** 855–8

[6] Nazikian R *et al* 1996 High-frequency core localized modes in neutral beam heated plasmas on TFTR *Phys. Plasmas* **3** 593

[7] Nguyen C *et al* 2009 Excitation of beta Alfvén eigenmodes in Tore-Supra *Plasma Phys. Control. Fusion* **51** 095002

[8] Smeulders P, Buratti P, De Benedetti M, Monari G and the FTU-Team 2002 Fast mhd analysis on ftu *Proc. 29th EPS Conf. on Plasma Physics and Controlled Fusion* (*Montreux, Switzerland, 2002*) vol 26B

[9] Buratti P, Smeulders P, Zonca F, Annibaldi S V, De Benedetti M, Kroegler H, Regnoli G, Tudisco O and the FTU-Team 2005 *Nucl. Fusion* **45** 1446–50

[10] Buratti P, Zimmermann O, De Benedetti M, Liang Y, Koslowski H R, Regnoli G, Smeulders O and Zonca F 2005 Inter-machine scaling of Alfvén-like modes excited by magnetic islands in FTU and TEXTOR *Proc. 32nd EPS Conf. on Plasma Physics* (*Tarragona, Spain, 2005*) vol 29C

[11] Zimmermann O, Koslowski H R, Krämer-Flecken A, Liang Y, Wolf R and the TEC-Team 2005 Coupling of Alfvén-like modes and large 2/1 tearing modes at TEXTOR *Proc. 32nd EPS Conf. on Plasma Physics* (*Tarragona, Spain, 2005*) vol 29C

[12] Annibaldi S V, Zonca F and Buratti P 2007 Excitation of beta-induced Alfvén eigenmodes in the presence of a magnetic island *Plasma Phys. Control. Fusion* **49** 475–83

[13] Lauber Ph, Brüdgam M, Curran D, Igochine V, Sassenberg K, Güunter S, Maraschek M, Garcí-Munoz M, Hicks N and the ASDEX Upgrade Team 2009 Kinetic Alfvén eigenmodes at ASDEX Upgrade *Plasma Phys. Control. Fusion* **51** 124009

[14] Guimarães-Filho Z O *et al* 2011 Eneregtic particle driven magnetohydrodynamic instabilities during relaxation cycles in Tore Supra *Plasma Phys. Control. Fusion* **53** 074012

[15] Chen W *et al* and the HL-2A Team 2010 Beta induced Alfvén eigenmodes destabilized by energetic electrons in a tokamak plasma *Phys. Rev. Lett.* **105** 185004

[16] Blackwell B D *et al* 2009 Configurational effectson Alfvénic modes and confinement in the H-1NF Heliac (arXiv:0902.4728v1)

[17] Ryu C M, Woo M H, Hole M J, Bak J K and the NFRI operation Team 2010 Observation and analysis of a high frequency MHD activity during sawteeth in KSTAR tokamak *23rd IAEA Fusion Energy Conf.* (*Daejeon, Korea, October 2010*)

[18] Hole M J, Ryu C M, Woo M H, Toi K, Kim J and Bak J G 2012 Analysis of Alfvén wave activity in KSTAR plasmas *24th IAEA Fusion Energy Conf.* (*San Diego, CA, October 2012*)

[19] Appel L C, Hole M J, Akers R J, Pinches S D and the MAST team 2002 Modelling of Alfvénic activity in the MAST tokamak *Proc. Joint Varenna–Lausanne Int. Workshop on the Theory of Fusion plasmas* (*Varenna, Italy, August 2002*)

[20] Sharapov S E *et al* and the JET-EFDA Contributors 2006 Alfvén cascades in JET discharges with NBI-heating *Nucl. Fusion* **46** S868–79

[21] Gorelenkov N N, Van Zeeland M A, Berk H L, Crocker N A, Darrow D, Fredrickson E, Fu G-Y, Heidbrink W W, Menard J and Nazikian R 2009 Beta-induced Alfvén-acoustic eigenmodes in National Spherical Torus Experiment and DIII-D driven by beam ions *Phys. Plasmas* **16** 056107

[22] Zonca F, Chen L and Santoro R A 1996 Kinetic theory of low-frequency Alfvén modes in tokamaks *Plasma Phys. Control. Fusion* **38** 2011–28

[23] Lee S G, Bak J G, Nam U W, Moon M K, Shi Y, Bitter M and Hill K 2010 The first experimental results from x-ray imaging crystal spectrometer for KSTAR *Rev. Sci. Instrum.* **81** 10E506

[24] Lutjens H, Bondeson A and Sauter O 1996 The CHEASE code for toroidal MHD equilibria *Comput. Phys. Commun.* **97** 219–60

[25] Poedts S and Schwartz E 1993 Computation of the ideal-MHD continuous spectrum in axisymmetric plasmas *J. Comput. Phys.* **105** 165–8

[26] Chapman I T, Sharapov S E, Huysmans G T A and Mikhailovskii A B 2006 Modeling the effect of toroidal plasma rotation on drift-magnetohydrodynamic modes in tokamaks *Phys. Plasmas* **13** 062511

[27] Nam Y U and Lee K D 2008 A 280 GHz single-channel millimeter-wave interferometer system for KSTAR *Rev. Sci. Instrum.* **79** 10E705

[28] Hole M J *et al* and the MAST Team 2005 Ideal MHD stability of the Mega-Ampere Spherical Tokamak *Plasma Phys. Control. Fusion* **47** 581–613

[29] Turnbull A D, Strait E J, Heidbrink W W, Chu M S, Duong H H, Greene J M, Lao L L, Taylor T S and Thompson S J 1993 Global Alfvén modes: theory and experiment *Phys. Fluids* B **5** 2456–553

[30] Huysmans G T A, Kerner W, Borba D, Holties H A and Goedbloed J P 1995 Modeling the excitation of global Alfvén modes by an external antenna in the Joint European Torus (JET) *Phys. Plasmas* **2** 1605–13

[31] Heidbrink W W 1982 Basic physics of Alfvén instabilities driven by energetic particles in toroidally confined plasmas *Phys. Plasmas* **15** 055501

[32] Zonca F, Chen L, Dong J Q and Santoro R A 1999 Existence of ion temperature gradient driven shear Alfvén instabilities in tokamaks *Phys. Plasmas* **6** 1917–24

[33] Bertram J, Blackwell B D and Hole M J 2012 Ideal-magnetohydrodynamic theory of low-frequency Alfvén waves in the H-1 Heliac *Plasma Phys. Control. Fusion* **54** 055009

[34] Berk H L, Van Dam J W, Guo Z and Lindberg D M 1992 Continuum damping of low-n toroidicity induced shear Alfvén eigenmodes *Phys. Fluids* B **4** 1806

[35] Zonca F and Chen L 1992 Resonant damping of toroidicity-induced shear-Alfvén eigenmodes in tokamaks *Phys. Rev. Lett.* **68** 592–5